Cerebral Cortex July 2015;25:1970–1980
doi:10.1093/cercor/bhu006
Advance Access publication February 10, 2014

Diffusion MR Microscopy of Cortical Development in the Mouse Embryo

Manisha Aggarwal[1], Ilan Gobius[2], Linda J. Richards[2,3] and Susumu Mori[1,4]

[1]Russell H. Morgan Department of Radiology and Radiological Science, Johns Hopkins University School of Medicine, Baltimore, MD, USA, [2]Queensland Brain Institute, [3]School of Biomedical Sciences, The University of Queensland, Brisbane, Queensland, Australia and [4]F.M. Kirby Research Center for Functional Brain Imaging, Kennedy Krieger Institute, Baltimore, MD, USA

Address correspondence to Manisha Aggarwal, Traylor Building, Room 334, Johns Hopkins University School of Medicine, 720 Rutland Avenue, Baltimore, MD 21205, USA. Email: maggarw2@jhu.edu

Cortical development in the mouse embryo involves complex changes in the microstructure of the telencephalic wall, which are challenging to examine using three-dimensional (3D) imaging techniques. In this study, high-resolution 3D diffusion magnetic resonance (dMR) microscopy of the embryonic mouse cortex is presented. Using diffusion-weighted gradient- and spin-echo based acquisition, dMR microimaging data were acquired from fixed mouse embryos at 7 developmental stages from embryonic day (E)12.5 to E18.5. The dMR imaging (dMRI) contrasts revealed microscopic structural detail in the mouse telencephalic wall, allowing delineation of transient zones in the developing cortex based on their unique diffusion signatures. With the high-resolution 3D data of the mouse embryo, we were able to visualize the complex microstructure of embryonic cerebral tissue and to resolve its regional and temporal evolution during cortical formation. Furthermore, averaged dMRI contrasts generated via deformable registration revealed distinct spatial and temporal gradients of anisotropy variation across the developing embryonic cortical plate and the ventricular zone. The findings of this study demonstrate the potential of 3D dMRI to resolve the complex microstructure of the embryonic mouse cortex, and will be important for investigations of corticogenesis and its disruption in embryonic mouse models.

Keywords: cortex, development, diffusion MRI, microimaging, mouse embryo

Introduction

Development of the cerebral cortex involves highly complex yet precisely ordered processes in the fetal telencephalic wall. The developing cortex is characterized by transient laminar zones (Rakic 1982; Kostovic et al. 2002), some of which begin to disappear by late gestation and lack direct counterparts in the adult brain. During corticogenesis, neurons proliferate primarily in the germinal ventricular zone (VZ) and undergo migration along the radial glial cell scaffold through the overlying intermediate zone (IZ) to form the cortical plate (CP), following an inside-out gradient (Rakic 1972; Sidman and Rakic 1973; Bayer and Altman 1991). In the laboratory mouse, because of the short gestation period, developmental changes in the embryonic cortex are especially rapid. The short gestation period and our ability to manipulate the mouse genome make it a useful experimental model to study mammalian cortical development.

The majority of corticogenesis in the mouse is known to proceed from about embryonic day 11 (E11) and continues until the end of gestation (Dehay and Kennedy 2007). During this time, the widening telencephalic wall undergoes drastic developmental changes at different stages, with continued migration of neurons from the ventricular epithelial zone to the overlying CP, to establish the laminar structure of the developing cortex (Angevine and Sidman 1961; Austin and Cepko 1990). Regional differences have been reported in the timing of major developmental events, including neuronal proliferation and migration, the appearance and growth of the cell-dense CP, and the establishment of long-range axonal connections (Smart and McSherry 1982). While cortical development in the mouse has been largely examined using different histochemical staining methods, the ability to visualize cortical microstructure in the intact mouse embryo with three-dimensional (3D) imaging has the potential to benefit studies examining corticogenesis and its disruption in developmental mouse models.

Currently, there are few available imaging techniques that allow obtaining 3D structural information from the embryonic mouse brain, and recent efforts are increasingly being made in this direction. Among the existing 3D imaging modalities, optical methods such as light sheet-based fluorescence microscopy techniques provide superior resolution for imaging of labeled cells or tissues in intact mouse embryos, that have been rendered optically transparent by the use of chemical tissue-clearing procedures (Dodt et al. 2007). A recent study has also shown the feasibility of electrophoretic tissue clearing using hydrogel-tissue hybridization (Chung et al. 2013), which in combination with optical imaging methods was applied to cellular resolution imaging of the adult mouse brain tissue. Currently, existing optical imaging hardware represents the main limiting factor for maximizing the relative depth of tissue penetration in optical imaging studies (Chung et al. 2013), which could be further enhanced with the development of specialized optics. More macroscopically, micro-computed tomography has been effectively used for anatomical imaging and phenotyping of mouse embryos (Wong et al. 2012), but it provides relatively homogeneous tissue contrast for delineation of structures within the brain. In comparison, among 3D magnetic resonance imaging (MRI) techniques, diffusion-weighted MRI uses an endogenous contrast generation mechanism (Beaulieu 2002) to provide distinct structural orientation-specific contrasts in nervous tissue, which can potentially be exploited for imaging of developing cortical microstructure in the embryonic mouse brain.

Diffusion MRI (dMRI), which measures the orientational properties of tissue water diffusion, is an effective technique to probe the anatomy of the developing mouse brain (Turnbull and Mori 2007). By measuring the properties of water diffusion that are determined by surrounding structural barriers in brain tissue, such as cellular membranes and myelin sheaths, dMRI renders image contrasts that can be used to infer the underlying complex tissue microstructure. While dMRI is

typically suited for imaging of white matter structures in nervous tissue, the cortical gray matter in the prenatal brain has been shown to exhibit high diffusion anisotropy, in humans (McKinstry et al. 2002; Huang et al. 2009; Xu et al. 2014), primates (Kroenke et al. 2005, 2007), and rodents (Zhang et al. 2003). The microstructural organization and distinct neuronal migration patterns in the fetal brain, involving the radial migration of neurons along processes of the transient radial glial scaffold and the tangential migration of neurons generated in the subpallial ganglionic eminences, form the basis of structural coherence in the developing cortex (Kolasinski et al. 2013). Although dMRI has been increasingly used for anatomical imaging of the developing mouse brain (Jacobs et al. 1999; Mori et al. 2001; Baloch et al. 2009), the application of dMRI to examine cortical microstructure in the embryonic brain remains difficult, owing to the limitation on imaging resolution. Given that the telencephalic wall in the embryonic mouse brain is an exceedingly thin layered structure (~0.1–0.3 mm thick at mid-gestation), ultra high-resolution imaging is vital in order to be able to resolve the emerging laminar zones and cortical microstructure in the mouse embryo.

In this work, we demonstrate high-resolution dMR microscopy for 3D imaging of the embryonic mouse cortex. Using diffusion-weighted gradient- and spin-echo based acquisition (Aggarwal et al. 2010), 3D microimaging data at a resolution of 52 µm isotropic were acquired from fixed embryonic brains at 7 developmental stages from E12.5 to E18.5, the peak of corticogenesis in the mouse. The high-resolution dMRI data could reveal microstructural detail in the embryonic cortex, allowing examination of the evolving embryonic zones in the cerebral wall during development. Regional changes in cortical microstructure were further examined with averaged maps of diffusion anisotropy at each stage of corticogenesis, to investigate the time course of cortical development and its regional variation in the embryonic mouse. The findings here will be useful for investigations of developmental phenotypes in mouse models of cortical malformation.

Materials and Methods

Specimens and Preparation

Embryonic stages were identified by designating the day of the appearance of a vaginal plug as embryonic day 0.5 (E0.5). A total of 21 embryos at 7 gestational stages (E12.5, E13.5, E14.5, E15.5, E16.5, E17.5, and E18.5; $n = 3$ at each stage) were used in this study. Embryos were obtained by euthanizing time-mated pregnant C57Bl/6 mice. Embryos E15.5 and older were perfusion-fixed with 0.9% saline, followed by 4% paraformaldehyde (PFA), and then post-fixed overnight in 4% PFA, while younger specimens were immersion-fixed using 4% PFA. The embryonic specimens were stored in PFA for over 4 weeks, and then transferred to phosphate-buffered saline with 3 mM gadopentetate dimeglumine (Gd-DTPA, Berlex Imaging, Wayne, NJ, USA) for 72 h to enhance the MR signal. For imaging, the specimens were embedded in 5% agarose gel (Sigma Aldrich, St Louis, MO, USA) with 3 mM Gd-DTPA, and placed in 10-mm diameter MR-compatible glass tubes. The tubes were filled with a perfluoropolyether liquid (Fomblin, Solvay Solexis, Thorofare, NJ, USA) for magnetic susceptibility matching. All animal procedures were approved by the Animal Use and Care Committee at the Johns Hopkins School of Medicine and the University of Queensland and were performed according to the Australian code of practice for the care and use of animals for scientific purposes.

Diffusion MR Microimaging

MR experiments were performed on a vertical-bore 11.7-T NMR spectrometer (Bruker Biospin, Billerica, MA, USA), with a Micro5.0 gradient system (maximum gradient strength = 3000 mT/m). A 10-mm diameter saddle coil was used as the radio frequency transmitter/receiver. At E12.5 and E13.5, whole mouse embryos were scanned since they were small enough to fit in 10-mm tubes, and excised embryonic heads were imaged at subsequent gestational stages. The temperature of the specimens was maintained at 37°C during imaging via the spectrometer's temperature control system. dMRI data were acquired using a 3D diffusion-weighted gradient- and spin-echo (DW-GRASE) sequence with navigator echo phase correction (Aggarwal et al. 2010), with the following imaging parameters: 4 refocusing pulses per repetition, 3 echoes acquired per refocusing pulse, echo time (TE)/repetition time (TR) = 34/650 ms, 4 signal averages, and bandwidth of 100 kHz. Twin navigator echoes were acquired at the end of each echo train, to monitor and compensate for phase modulation of the *k*-space data as described previously (Mori and van Zijl 1998). For each dataset, 18 independent diffusion-weighted directions (*b*-value ~1400 s/mm^2) and 2 additional images with minimal diffusion-weighting (*b*0) were acquired, with the diffusion gradient duration (δ)/separation (Δ) = 3.2/12 ms. The field of view (FOV) and acquisition matrix size ranged from $6.7 \times 6.4 \times 7.5$ to $8.7 \times 7.1 \times 10.3$ mm^3 and $128 \times 124 \times 144$ to $168 \times 136 \times 198$ for the E12.5–E18.5 specimens, respectively, for a native isotropic spatial resolution of $52 \times 52 \times 52$ µm^3. Images were acquired with fully sampled *k*-space data, which was zero-filled by a factor of 2 prior to Fourier transformation to a voxel-size of 26 µm isotropic. The total acquisition time was 21.5–32 h for the E12.5–E18.5 specimens. T_2-weighted images were acquired with the same FOV and resolution as the dMRI data, using a rapid acquisition with relaxation enhancement sequence, with a rare factor of 8, TE/TR = 40/1000 ms, and 4 signal averages.

Data Processing

Images were reconstructed from the 3D *k*-space data using IDL (ITT Visual Information Solutions, Boulder, AZ, USA). We used the tensor model of diffusion to compute quantitative anisotropy and orientation maps. From the dMR images, voxel-wise diffusion tensors were calculated using the Log-linear fitting function in DtiStudio (Jiang et al. 2006), from which parametric maps of fractional anisotropy (FA), primary eigenvector, and linear diffusion measure (CL) (Westin et al. 2002) were derived. Direction-encoded colormap (DEC) images were generated by combining the primary eigenvector and CL maps, with the ratio between the red, green, and blue components equal to the ratio of absolute values of components of the primary eigenvector, and the magnitude proportional to CL. Isotropically diffusion-weighted (iDW) images were calculated by averaging diffusion-weighted images along isotropically distributed directions.

Probabilistic streamline tracking (Behrens et al. 2003; Parker et al. 2003) based on the dMRI data was performed to generate super-resolution track-density imaging (TDI) maps (Calamante et al. 2011; Tournier et al. 2012) of the embryonic cortex. Fiber orientation distribution (FOD) functions were first estimated from the dMRI data using the constrained spherical deconvolution (CSD) method in MRtrix (Tournier et al. 2012). The maximum spherical harmonic order (*lmax*) for CSD was set to 4 for 18 diffusion directions. FOD-based probabilistic streamline tracking was performed using a step size of 0.002 mm, maximum angle between steps of 46°, minimum tract length of 0.15 mm, and an FOD amplitude threshold of 0.12 was used to terminate the tracking. To generate TDI maps of the cortex, a mask covering the telencephalic region was defined for each specimen, and approximately one million such streamlines were tracked to generate TDI maps of the cortex at a grid size of 4 µm isotropic.

Computation of Sample-Averaged Anisotropy Maps of the Embryonic Cortex

From 3D dMRI of individual embryonic specimens ($n = 3$ at each stage), we generated sample-averaged tensor data of whole mouse heads at each gestational stage, using an iterative process described previously (Aggarwal et al. 2009). This was done in order to minimize anatomical bias from individual embryonic specimens in the segmentation of cortical regions at each stage. The averaging procedure was based on initial linear affine registration (Woods et al. 1998) to the specimen with median volume at each stage, followed by iterative

2-channel (iDW and CL) large deformation diffeomorphic metric mapping (LDDMM; Miller et al. 2002) and averaging after each step. Nonlinear registration based on LDDMM was driven by both structural iDW and CL-based anisotropy contrasts, in order to ensure accurate registration of the overall brain and ventricular morphology and internal structures within the brain, respectively. In the final step of mapping, in order to exploit the rich anatomical contrast of the DEC maps, iDW and DEC-based orientation contrasts were used for multichannel (1 channel for iDW and 3 channels for DEC) LDDMM to minimize residual anatomic misalignment. The derived diffeomorphic transformations were applied for spatial normalization and reorientation of the tensor data using the methods described in Alexander et al. (2001), and from the averaged diffusion tensors, the FA, CL, primary eigenvector, and DEC maps at each embryonic stage were computed.

Segmentation of Cortical Regions in the Mouse Embryo

Based on the dMRI contrasts, the embryonic cerebral wall could be three-dimensionally segmented into the VZ, IZ, and CP at successive stages of corticogenesis. Semiautomated segmentation of the 3 layers was done based on direction-encoded colormap contrasts, using vector-seeded region growing in RoiEditor (www.mristudio.org). Using consistently identifiable landmarks at each gestational stage, the developing CP was further divided into 4 regions: (from medial to lateral), the hippocampal formation, the cingulate cortex, the neocortex, and the paleocortex ventral to the rhinal fissure. The lateroventral border of the neocortical plate was demarcated by the rhinal fissure. The border between the cingulate cortex and the neocortex was defined by a line from the medial corner of the lateral ventricle to the apex of the interhemispheric fissure. Segmentation of cortical regions was done based on the averaged DEC maps at each embryonic stage and was then propagated to individual specimens using the inverse of the diffeomorphic maps, for quantitative measurements of FA and regional volumes. Wilcoxon rank-sum tests were used for comparison of FA measurements across cortical regions. Statistical tests were performed using MATLAB (MathWorks, Natick, MA, USA).

Fluorescence Immunohistochemistry

Immunolabeling was performed on 50-μm thick horizontal vibratome sections processed for fluorescence immunohistochemistry as described previously (Plachez et al. 2008). Sections were mounted on slides and sodium citrate antigen retrieval was performed prior to incubation with primary antibodies. We identified radial glia using an antibody to GLAST, a glial-specific glutamate transporter, and an antibody to neuron-specific βIII-tubulin was used to label the microtubules of dendritic and axonal processes. Fluorescence was visualized with a donkey anti-rabbit Alexafluor555 (1 : 500; Invitrogen) and a biotinylated donkey anti-mouse IgG (1 : 500; Jackson ImmunoResearch) secondary antibody amplified with a Streptavidin–Alexafluor647 conjugate (1 : 500; Invitrogen). Primary antibodies used were: mouse anti-GLAST (or Eaat1; 1 : 500; ab49643, Abcam) and rabbit antineuronal-specific βIII-tubulin (1 : 500; ab18207, Abcam). Photomicrographs of stained sections were acquired as multiple image projections of approximately 20-μm thick *z*-stacks using an LSM 710 confocal microscope and Zen 2012 software (Carl Zeiss).

Results

Typical signal-to-noise ratio (SNR) values for dMR microimaging of the embryonic specimens at 52-μm isotropic resolution (measured in the cortical region in *b*0 images) were ~76 and ~87 at E12.5 and E18.5, respectively. Representative sagittal sections illustrating sample-averaged tensor contrasts from the mouse embryo at E12.5, the earliest time point examined here, are shown in Figure 1*A*,*B*. The resulting dMR microimaging data allowed detailed visualization of the embryonic cortical structure with high contrast and SNR.

dMR Microimaging of the Embryonic Cortex at E12.5–E13.5

Figure 2*A* compares structural T_2-weighted, iDW, and FA contrasts in the mouse telencephalon at E12.5. The FA maps at E12.5 revealed markedly high diffusion anisotropy in the region along the ventricular wall of the telencephalic vesicle (FA map in Fig. 2*A*), corresponding to the VZ of the embryonic cortex. In early corticogenesis, the VZ is characterized by elongated radial glial cells with dense processes that span the width of the developing cortex. The DEC maps at this stage revealed a single layer of high anisotropy along the ventricular margin, with the orientation of anisotropy seen to be radial to the pial surface (DEC maps in Fig. 2*B*). Probabilistic streamline tracking based on the dMRI data at E12.5 showed reconstruction of fine fascicles that were seen radiating perpendicular to the ventricular surface throughout the extent of the telencephalon, and traversed the entire thickness of the VZ at this stage (Fig. 2*C*). Twenty-four hours later (at E13.5), the appearance of a very thin CP could be resolved in DEC contrasts, appearing as a distinct layer at the

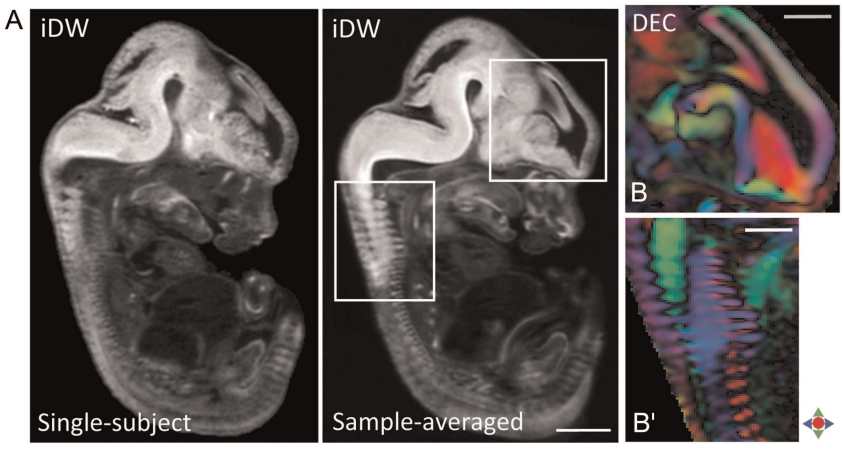

Figure 1. Representative sagittal sections from the E12.5 mouse embryo showing sample-averaged tensor contrasts in the embryonic brain. (*A*) Sagittal view shows iDW contrasts from single-subject (left) and sample-averaged (right) whole embryo images. (*B*–*B*′) Zoomed-in views of DEC images through select regions (in the forebrain and vertebral column, indicated by white boxes in *A*) illustrate the anatomical contrast and preservation of fine structural detail in the tensor-averaged orientation maps. Red: Medial-lateral; green: dorsal-ventral; blue: anterior-posterior. Scale bar for *A* = 1 mm, and for *B*–*B*′ = 0.5 mm.

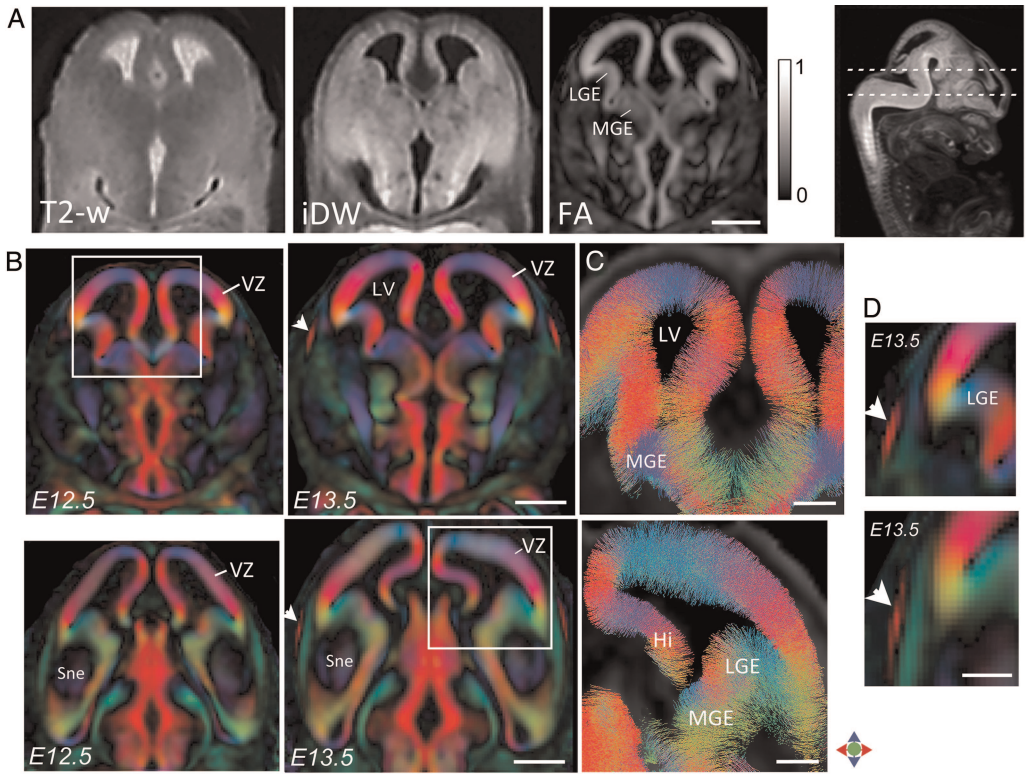

Figure 2. Diffusion MR microimaging of the embryonic mouse cortex at E12.5–E13.5. (*A*) Comparison of T_2-weighted, iDW, and FA contrasts in a horizontal section through the E12.5 telencephalon shows markedly high diffusion anisotropy in the VZ (FA map, scale of 0–1). (*B*) DEC contrasts reveal the radial orientation of anisotropy throughout the VZ at E12.5 and E13.5. The location of the sections is indicated in the sagittal iDW image at the top right. White arrowheads indicate the appearance of the CP resolved in DEC maps at E13.5. Magnified views through the lateral cerebral wall are shown in *D*, indicating the emerging CP delineated by its radially oriented anisotropy (arrowheads). (*C*) Probabilistic streamline tracking based on the dMRI data (regions indicated by white boxes in *B*) shows fine radially oriented processes spanning the entire width of the VZ at E12.5 (top) and E13.5 (bottom). Fibers displayed in *C* are cropped to a horizontal slab of 0.1 mm thickness. Color indicates the local orientation (red: medial-lateral; green: dorsal-ventral; blue: anterior-posterior). Hi: hippocampal neuroepithelium; MGE: medial ganglionic eminence; LGE: lateral ganglionic eminence; LV: lateral ventricle; Sne: striatal neuroepithelium; VZ: ventricular zone. Scale bars for *A*–*B* = 0.5 mm and for *C*–*D* = 200 μm.

lateral-most aspects of the cerebral wall (white arrows in Fig. 2*B*,*D*). The emerging CP could be clearly distinguished from the underlying IZ in DEC maps at E13.5, by its predominantly radially oriented anisotropy.

Transient Embryonic Zones in the Cerebral Wall Delineated with dMR Microimaging at E14.5–E15.5

By E14.5, 3 layers with distinct anisotropy patterns could be delineated in the embryonic cerebral wall in DEC maps (Fig. 3). The developing CP and the VZ were characterized by high anisotropy oriented radial to the pial surface, and the IZ between these 2 layers showed structural orientation predominantly tangential to the pial surface (DEC maps in Fig. 3*A*). At E14.5, the developing CP could be resolved throughout the lateral wall of the telencephalon. In comparison, formation of the CP in medially located regions of the telencephalon was found to occur at a relatively delayed interval, starting at E15.5. This can be clearly seen in DEC sections through the hippocampal formation (Fig. 3*B*,*C*), that reveal the appearance of a distinct hippocampal CP (hCP) at E15.5 (white arrowheads in Fig. 3*B*), which could not be distinguished from the underlying VZ at E14.5. The subplate, identified as a thin region of relatively low anisotropy between the IZ and CP, can also be seen in the hippocampal sections at E14.5–E15.5 (Fig. 3*C*). Figure 3*D* shows the FODs estimated from spherical deconvolution of dMRI data in the E14.5 cortex, which showed layer-specific structural orientations in the developing CP and the transient IZ and VZ (Fig. 3*D*). Reconstruction of fiber tracks in the cerebral wall at E14.5 revealed densely packed radial processes inclined orthogonal to the ventricular surface throughout the VZ (Fig. 3*E*), while a predominantly tangential orientation of fibers running parallel to the pial surface was evident in the IZ as well as in the lateral ganglionic eminence (LGE). Streamline tractography at this stage also revealed the reconstruction of very fine radially oriented processes in the CP, which traversed at right angles to the IZ fibers and could be resolved extending across the width of the CP to the pial surface (shown in Fig. 3*E*).

Evolving Cortical Microstructure During Embryonic Development Resolved with dMRI

By E16.5, the CP could be delineated extending throughout the neocortical and hippocampal surface in DEC contrasts (Fig. 4). From E16.5 to E18.5, a drastic growth of the CP along the entire cortical surface was seen in DEC maps, with a concomitant decrease observed in the thickness of the VZ (Fig. 4*A*). FA and DEC contrasts also revealed a progressive decline in diffusion anisotropy in the VZ during this period (Fig. 4*A*,*B*). This loss of structural coherence in the VZ is further illustrated using the track-density imaging (TDI) technique (Fig. 4*C*), which renders fiber tracking results at a resolution higher than the native imaging resolution and provides subvoxel

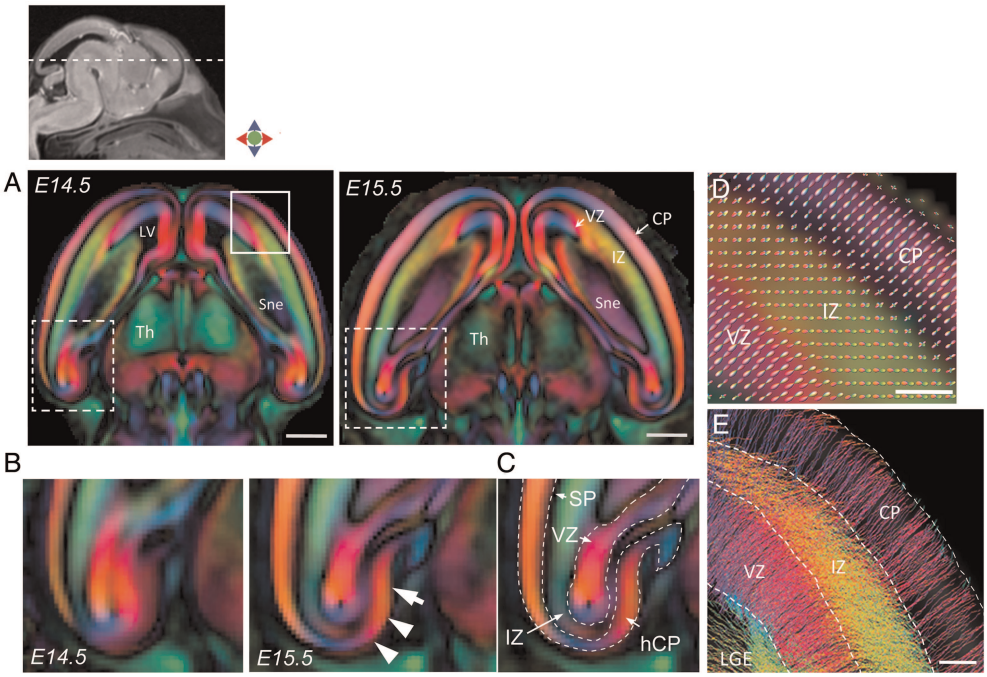

Figure 3. Delineation of the VZ, IZ, and developing CP with dMR microimaging at E14.5–E15.5. (*A*) Horizontal DEC sections through the telencephalon at E14.5 (left) and E15.5 (right) show distinct patterns of anisotropy in the embryonic cerebral wall, with radial orientation in the VZ and CP, and predominantly tangential orientation in the IZ. (*B–C*) Comparison of DEC sections through the hippocampal formation at E14.5 and E15.5 (areas indicated by dashed white boxes in *A*) shows the appearance of a distinct hCP at E15.5 (white arrows). Structural boundaries of the VZ, IZ, and hCP resolved from the DEC contrasts at E15.5 are overlaid in *C*. (*D*) High-magnification view of a section through the lateral cerebral wall at E14.5 (corresponding to the region within the solid white box in *A*) shows the fiber orientation distributions estimated from the dMRI data overlaid on the DEC map. (*E*) Probabilistic tractography shows fine radially oriented processes reconstructed in the VZ and the CP at E14.5, with predominantly tangential orientation of fibers seen in the IZ and also in the LGE. LV: lateral ventricle; Sne: striatal neuroepithelium; SP: subplate; Th: thalamus. Scale bars for *A* = 0.5 mm, and for *D–E* = 100 μm.

visualization of tissue microstructure. The TDI section through the embryonic cortex at E18.5 (Fig. 4*C*) demonstrates a strong radially arranged pattern in the gray matter of the CP, with relatively less well-defined structural alignment evident in the VZ at this stage. The tangential structural orientation of the IZ located between the CP and the VZ can also be seen in Figure 4*C*. For comparison, cortical sections immunostained for GLAST and βIII-tubulin in the E17.5 embryo are shown in Figure 5. A well-defined radial organization of the radial glial scaffold is evident in the GLAST-immunostained section in Figure 5*A*. Labeling for neuron-specific βIII-tubulin illustrates the radial orientations of neuronal processes in the developing CP, as well as tangentially oriented fibers in the IZ at this stage (Fig. 5*B*,*C*).

TDI maps through the lateral telencephalic wall from E12.5 to E18.5 revealed the evolving cortical microstructure during the embryonic period (Fig. 6). At E12.5, the TDI sections clearly showed 2 separate developmental zones, the VZ with radially oriented microstructure (red in the TDI maps), and an outer layer with low structural coherence corresponding to the primordial plexiform layer and incipient IZ. At E13.5, the early emerging CP could be seen, splitting this outer layer into a superficial marginal zone (MZ) and the deeper IZ. The appearance of the very thin CP as a distinct layer (distinguished by its radially oriented structure) between the MZ and IZ could be clearly resolved in TDI sections at E13.5 and is shown in Figure 6. In comparison, the superficial MZ, which contains horizontally oriented bipolar cells and axonal fibers, showed structural organization primarily parallel to the pial surface. TDI maps in later fetal stages (after E16.5) revealed progressive loss of the well-defined radial microstructure in the VZ (hypointense regions in the VZ at E17.5–E18.5 in Fig. 6). In the IZ, both radially and tangentially oriented processes could be resolved apposed orthogonally in the TDI sections at E14.5–E15.5. At subsequent embryonic stages, the TDI maps showed thickening of the IZ with tangentially oriented fibers, corresponding to the orientation of early efferent and afferent axons that infiltrate the IZ during this period. These fibers were delineated as tangentially oriented criss-crossing processes in the IZ, and could be resolved as they innervated the gray matter of the CP in TDI contrasts at E17.5–E18.5 (Fig. 6).

Delineation of Developing Callosal Connections with dMRI Contrasts

Medially, the IZ was infiltrated by callosal axons that could be resolved projecting to the midplane between E16.5 and E18.5. Figure 7 shows the delineation of developing callosal projections in DEC contrasts at E18.5. In the body of the corpus callosum (cc), callosal fibers were resolved crossing the midplane in a thin bundle just dorsal to and adjoining the hippocampal commissure (hc), and could be delineated from the hc fibers by the interposed hippocampus with orthogonally oriented anisotropy in DEC sections (Fig. 7*B*,*C*). More caudally, callosal projections had not crossed the midplane at E18.5 and were resolved forming a bundle of medially oriented projections in the IZ bilateral to the midline in DEC sections (Fig. 7*D*,*D′*). The outgrowth of callosal fibers in the splenium of the cc approaching the midline can be clearly seen in DEC maps in Figure 7*D*, indicating a rostro-caudal difference in the developmental timing of callosal connections in the embryonic cortex.

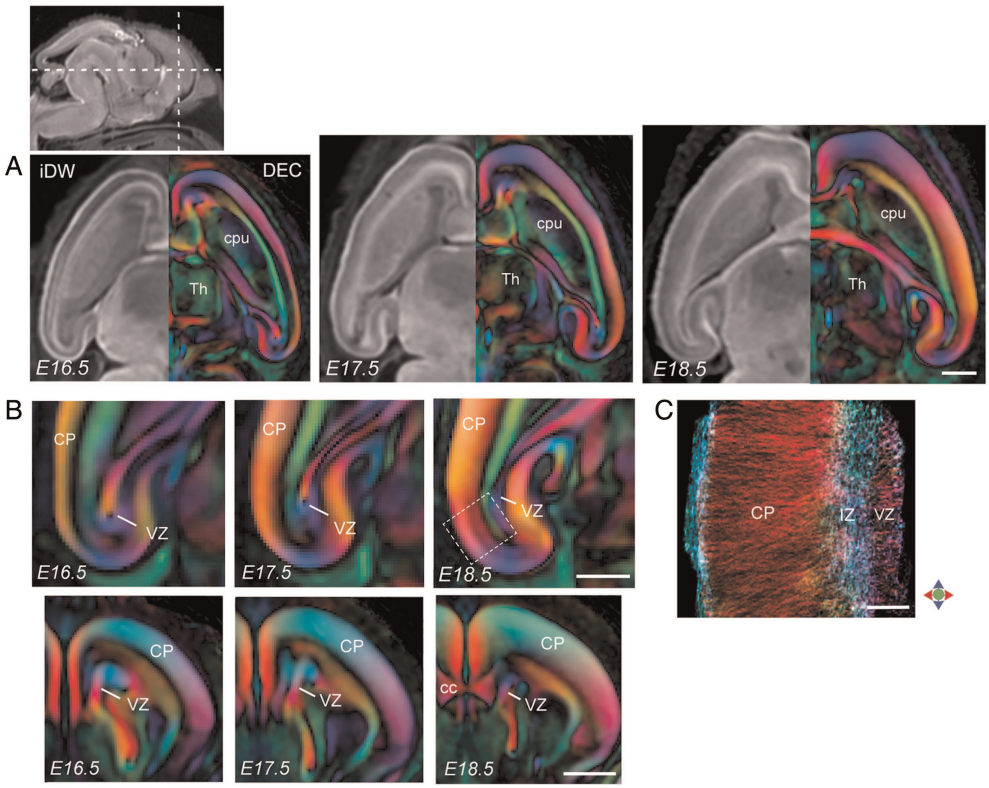

Figure 4. dMR microimaging of the embryonic mouse cortex from E16.5 to E18.5. (*A*) Horizontal sections through the telencephalon at E16.5, E17.5 and E18.5 show the radial pattern of anisotropy and increasing thickness of the CP with gestational age. iDW and DEC contrasts are shown in the left and right hemi-sections, respectively. (*B*) Magnified views of horizontal sections through the hippocampal formation (top panel) and coronal sections through the forebrain (bottom panel) show temporal changes in the thickness of the developing CP and the VZ resolved with DEC contrasts. The anatomical locations of the sections are indicated by dashed lines in the sagittal iDW image at the top left. (*C*) High-resolution track-density image of a small region through the cerebral wall at E18.5 (corresponding to the area within the dashed white box in *B*) reveals the radially arranged microstructure of cortical gray matter in the CP resolved with dMR microimaging. Color represents the local orientation of anisotropy (red: medial-lateral; green: dorsal-ventral; blue: anterior-posterior). cc: corpus callosum; cpu: caudoputamen; Th: thalamus. Scale bars for *A–B* = 0.5 mm and for *C* = 100 μm.

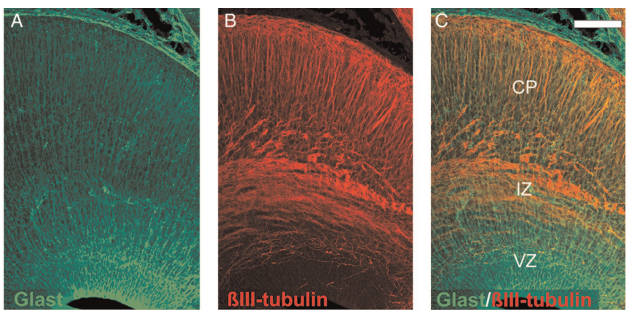

Figure 5. Fluorescence immunohistochemistry of the embryonic cortical wall at E17.5. Horizontal sections immunolabeled with antibodies to GLAST (*A*) and βIII-tubulin (*B*) reveal the organization of the radial glial scaffold and axonal and dendritic processes in the embryonic cortex at E17.5. The radial and tangential orientation of processes in the VZ, CP, and IZ can be seen in the merged image (*C*). Scale bar = 100 μm.

Regional Variation in Cortical Anisotropy During Embryonic Development

Figure 8 shows quantitative mapping of FA measurements from the averaged tensor data of embryonic stages. A distinctly heterogeneous time course of variation in anisotropy along the cortical surface was observed from E12.5 to E18.5. In the CP, a lateral-medial and rostral-caudal gradient of FA increase was detected following its appearance at E13.5 (Fig. 8). FA in the VZ exhibited a reverse gradient, decreasing progressively along the latero-medial axis (Fig. 8, bottom panel). A sharp transition in FA was evident at the lateral cortical surface (indicated by white arrows in Fig. 8), which was anatomically coincident with the rostro-caudal extent of the rhinal fissure that marks the transition between the 6-layered neocortex and the paleocortex in the mature brain (black dashed line in Fig. 8).

From the dMR microimaging data, regions of the embryonic cortex could be three-dimensionally reconstructed with structural detail (Fig. 9*C*,*D*). Plots of volume versus gestational age revealed a drastic increase in the volume of the CP between E13.5 and E18.5 (Fig. 9*A*). The volume of the neuroepithelial VZ showed an increase in the early phase of corticogenesis (up to E14.5) and progressively declined thereafter (inset in Fig. 9*A*). The mean FA in the developing CP was found to show a monotonic increase throughout the gestational period, with the highest value (0.46 ± 0.03) at E18.5. In the VZ, the FA increased monotonically reaching a peak (0.47 ± 0.02) at E16.5, and then declined (Fig. 9*B*). The VZ exhibited higher FA compared with the CP up to E16.5, and after E16.5 this contrast was reversed, with FA in the VZ being significantly ($P < 0.005$) lower compared with FA in the CP at E18.5 (Fig. 9*B*). Significant differences in the time course of FA variation were also observed in different areas of the developing CP along its

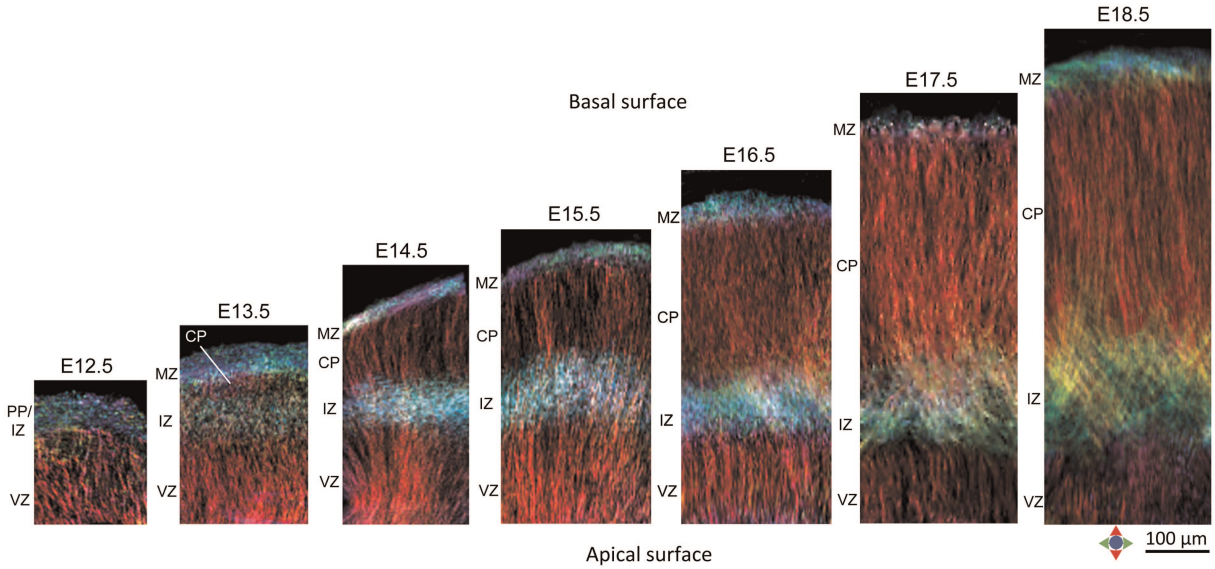

Figure 6. TDI maps of the cerebral wall in the mouse embryo from E12.5 to E18.5. TDI sections in the coronal plane from the lateral region of the telencephalic wall at each developmental stage, generated at a grid size of 4 μm isotropic from the dMRI data, are shown. The TDI maps reveal the distinct developmental zones in the cerebral wall and their evolving microstructure at successive stages of corticogenesis. CP: cortical plate; IZ: intermediate zone; MZ: marginal zone; PP: primordial plexiform layer; VZ: ventricular zone. Color represents the local orientation of anisotropy (red: medial-lateral; green: dorsal-ventral; blue: anterior-posterior). Scale bar = 100 μm.

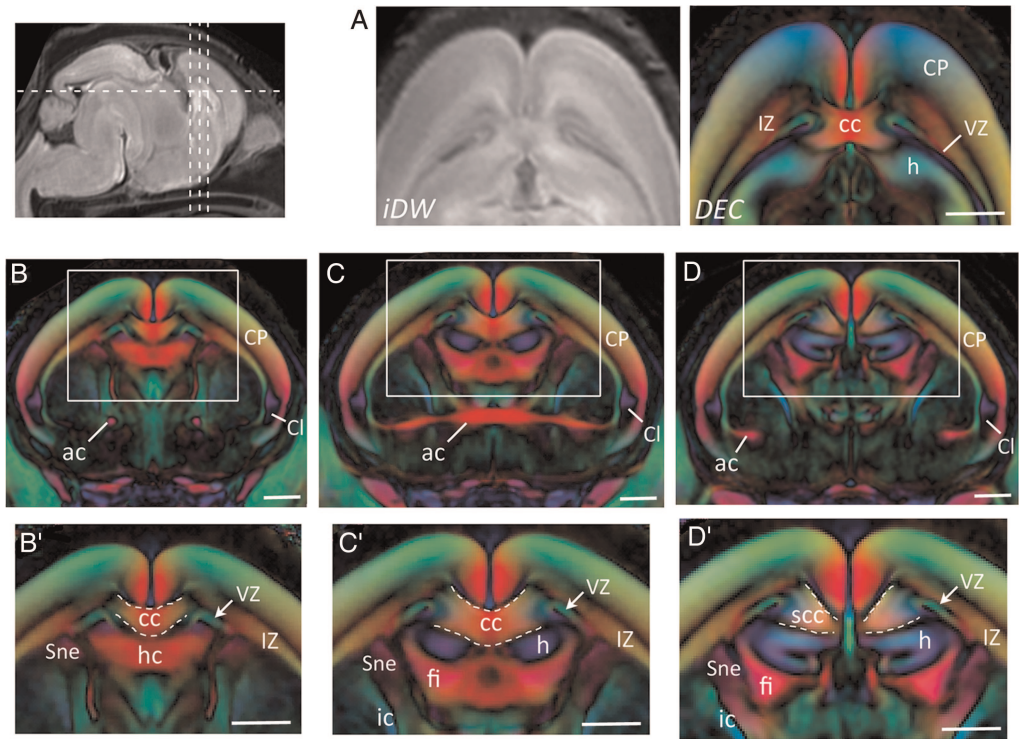

Figure 7. Delineation of developing callosal connections in the E18.5 mouse cortex. (*A*) Horizontal sections through sample-averaged iDW and DEC maps of the telencephalon show the embryonic cc resolved in DEC contrasts. (*B–D*) Coronal DEC views through the forebrain (along the dashed lines in the iDW image at the top left) reveal the telencephalic commissures delineated at E18.5. (*B′–D′*) Magnified views of the dorsal telencephalic region (areas within the white boxes in *B–D*) show the delineation of developing callosal fibers, at the level of the body (*B′–C′*), and the splenium (*D′*) of the cc. ac: anterior commissure; cc: corpus callosum; Cl: claustrum; fi: fimbria; h: hippocampus; hc: hippocampal commissure; scc: splenium of the cc; Sne: striatal neuroepithelium. Scale bars = 0.5 mm.

latero-medial axis (Fig. 9*E–H*). The paleocortex showed significantly ($P < 0.005$) low FA compared with the neocortex at the developmental time points examined here (Fig. 9*E*,*G*). In medial regions of the developing CP, that is, the cingulate cortex and the hippocampal formation, a temporal lapse in FA profiles with gestational age could be observed compared with the neocortical plate (Fig. 9*F*,*H*), consistent with a latero-medial gradient of FA increase across the CP.

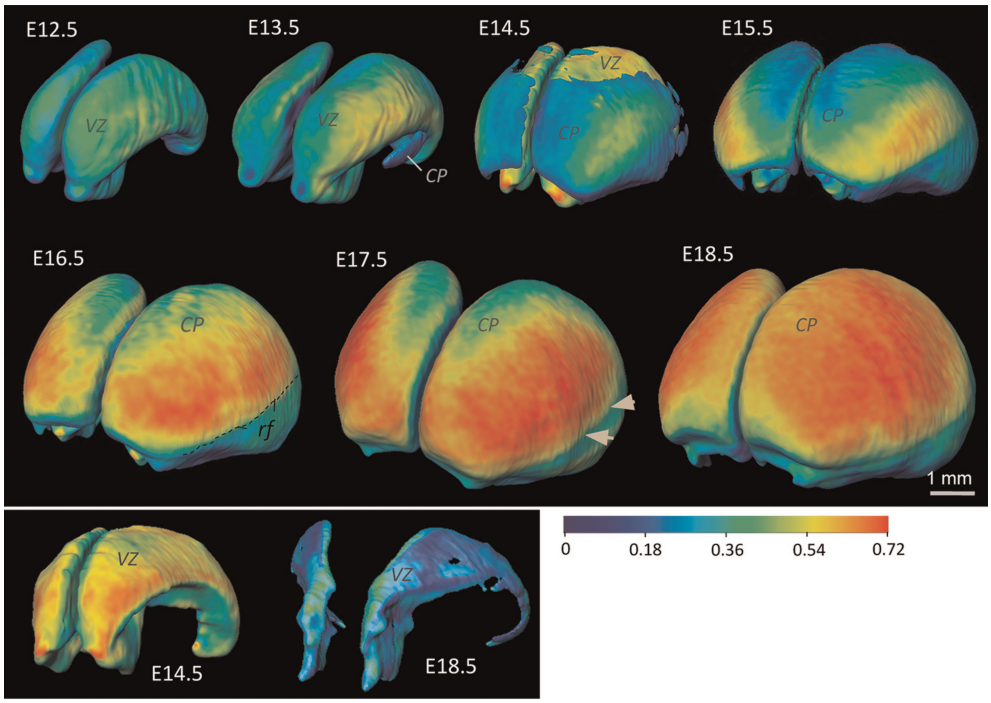

Figure 8. Cortical surface mapping of FA values in the embryonic mouse brain from E12.5 to E18.5. Color represents FA measurements from sample-averaged tensor data ($n = 3$) at each stage as shown in the color bar. White arrowheads indicate the marked transition in cortical FA seen along the rostro-caudal extent of the rhinal fissure (indicated by the black dashed line at E16.5) separating the neocortex and the paleocortex. The bottom panel shows the comparison of surface FA in the VZ at E14.5 (left) and E18.5 (right), indicating a drastic decrease in FA in the VZ with gestational age.

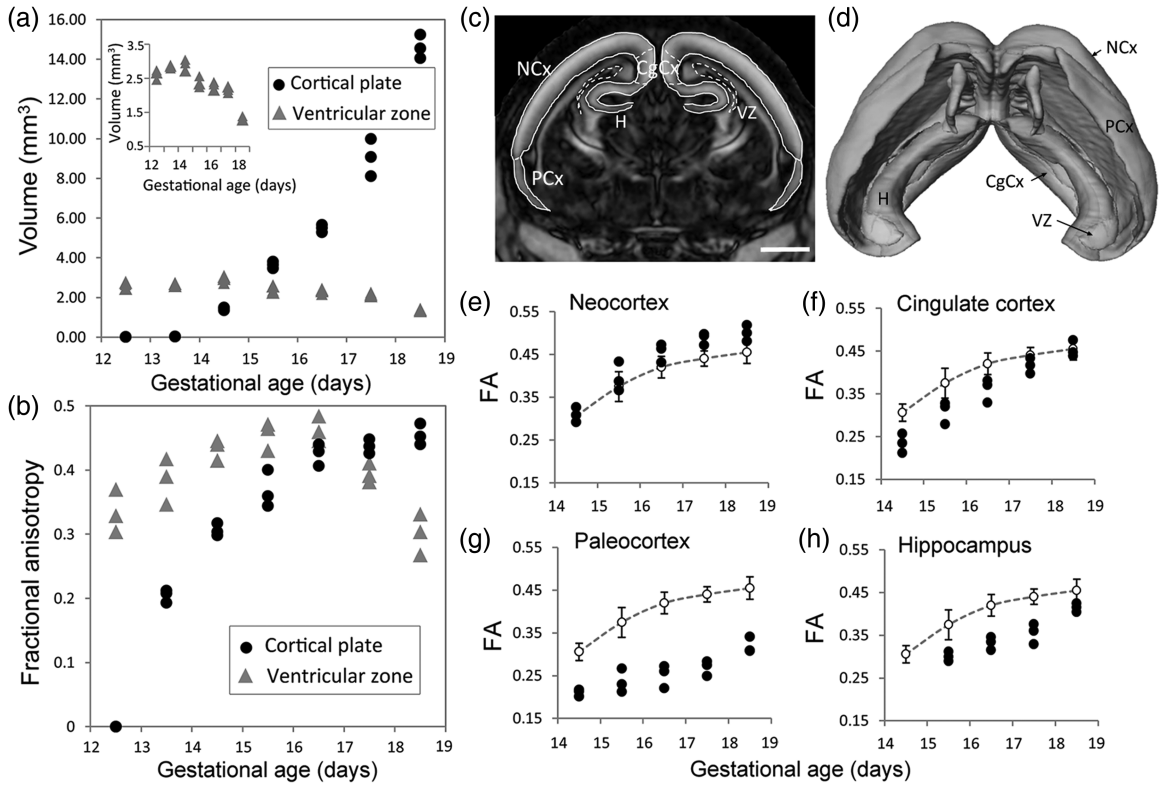

Figure 9. Regional changes in cortical anisotropy during embryonic development. (*A*) Plot showing the change in regional volumes of the VZ and CP with gestational age. Data points are volume measurements from embryonic specimens ($n = 3$) at each stage. The plot in the inset shows the VZ volume with the *y*-axis scaled to illustrate the temporal variation. (*B*) FA in the VZ and the CP plotted versus gestational age. Data shown are mean FA measurements over the VZ and the CP from embryos ($n = 3$) at each stage. (*C–D*) Representative coronal section from an E18.5 embryo showing structural boundaries of cortical regions overlaid on the FA map, with 3D surface rendering of the segmented regions shown in *D*. CgCx: cingulate cortex; H: hippocampal formation; NCx: neocortex; PCx: paleocortex. Scale bar = 1 mm. (*E–H*) Plots of regional FA measurements across the developing CP, in the neocortex (*E*), cingulate cortex (*F*), paleocortex (*G*), and the hippocampus (*H*). Dashed lines indicate the average FA profile over the entire CP, with error bars representing the standard deviation.

Discussion

This study demonstrated diffusion MR microscopy of cortical development in the mouse embryo, from 12.5 to 18.5 days post-conception. Using accelerated acquisition with a 3D GRASE sequence, dMR microimaging data at a resolution of 52 μm could be acquired with high SNR, which revealed fine microstructural detail in the embryonic mouse cortex. Developing and transient zones during corticogenesis, and the evolving microstructure of the embryonic cerebral wall, could be resolved and uniquely visualized with dMRI contrasts. We found that zones of the embryonic mouse cortex exhibit unique diffusion signatures, which reflect the underlying tissue microstructure and can reveal its spatio-temporal evolution during cortical maturation.

Cortical anisotropy in the fetal brain has been previously examined in studies using dMRI in humans and animal models. The existence of radially oriented diffusion anisotropy was reported in the cortex of preterm infants (McKinstry et al. 2002). Huang et al. (2009) have shown delineation of the fetal cerebral wall into 3 layers separated on the basis of FA contrasts. Recent reports have also examined radial and tangential coherence in the cerebral wall using postmortem imaging of fetal brains (Xu et al. 2014; Kolasinski et al. 2013). In primates and rodents, diffusion tensor imaging contrasts have been used to differentiate regions of the developing cortex (Zhang et al. 2003; Kroenke et al. 2007; Huang et al. 2008). Here, we showed that with high-resolution dMR microimaging, the complex structure of the embryonic mouse cerebral tissue could be resolved at microscopic levels, revealing the underlying radial and tangential cytoarchitecture of different cortical zones. The findings demonstrate the potential of high-resolution dMRI to probe cortical microstructure in the developing mouse brain three-dimensionally, and will be important for investigations of cortical malformation and related defects in embryonic mouse models. Moreover, these results demonstrate that from the earliest emergence of the CP, differences in TDI maps are evident between the VZ, containing radial glia whose processes are anchored at both the ventricular and pial surfaces (Noctor et al. 2001), and the preplate layer of differentiating neurons. Since dMRI and TDI contrasts were sensitive enough to detect even these small changes in diffusivity between the 2 layers, our results indicate that even very small differences in cell shape and process orientation of cell bodies in the VZ, compared with the preplate, may be observed with this technique.

As shown in Figure 2, using water diffusion as an endogenous probe, the developing CP (~80 μm thick) could be clearly resolved at its first appearance at E13.5. This observation is consistent with previous studies that have reported the emergence of the early CP between E13 and E14 in the mouse, using histological hematoxylin and eosin (H&E) staining (Smart and McSherry 1982; Smart 1983). Our findings showed increasing diffusion anisotropy in the CP throughout the embryonic period examined here, while a relative decrease in anisotropy in the VZ was observed in later embryonic stages (after E16.5, the plot in Fig. 9*B*). This temporal reversal in the relative anisotropy between the VZ and the CP coincides with the time course of underlying changes in cortical cytoarchitecture during development, with neuronal migration from the epithelial VZ into the developing CP as corticogenesis proceeds (Smart and McSherry 1982). The increased radial anisotropy and track density in the CP observed here (Figs 4*C* and 5) might reflect structural changes with the growth of neuronal apical dendrites that extend in clusters across the developing CP, as they reach toward the pial surface to establish end-feet at the MZ (Hirst et al. 1991). Furthermore, a progressive decline in the well-defined radial arrangement of the VZ could also be observed in the track-density images toward later embryonic stages (E17.5–E18.5, shown in Fig. 6). The late phase of corticogenesis (~E17.5 in the mouse) is marked by the disruption of the transient scaffold of radial glia, as neuronal proliferation and migration decline (Schmid et al. 2003; Kwan et al. 2012). Although the precise time course and cellular mechanisms that underlie the dismantling of the radial glial scaffold are not very well established, our findings suggest that a progressive decline in the radial structural organization could be detected in the VZ of the lateral cerebral wall, starting during later embryonic stages. These observations indicate that dynamic changes in the cerebral microstructure and its increasing complexity at different stages of corticogenesis in the mouse could be sensitively captured with dMR microimaging.

With probabilistic tracking based on spherical deconvolution, we were able to reconstruct microscopic radial processes in the embryonic mouse cortex (Figs 2 and 3), which closely reflect the spatial arrangement of processes of radial glial cells shown with microtubule-associated protein 2 immunostaining (Del Rio et al. 2000). Using the super-resolution track-density imaging technique, the microstructure of embryonic cortical zones could also be visualized in further detail. TDI contrasts in the mature mouse brain have been shown to correlate with histological staining before (Calamante et al. 2012). Here, we showed that TDI of cortical gray matter in the embryonic brain revealed the microscopic radial array of glial fibers in the VZ and the developing CP, and the tangentially arrayed structure of the IZ and the MZ. Infiltration of the IZ with tangentially oriented fibers in later embryonic stages, and their innervation of cortical gray in the CP, could also be resolved with TDI contrasts and agrees with the developmental time course of early efferent and afferent fibers in the mouse brain (Del Rio et al. 2000). Similarly evolving cerebral microstructure in sections of the mouse telencephalic wall has been reported in previous studies, using thymidine autoradiography and histological sectioning at successive embryonic time points (Smart and McSherry 1982; Miyama et al. 1997; Dehay and Kennedy 2007). Certain features, however, such as the narrow subventricular zone, which reflects a difference in cellular morphology and peptide expression compared with the underlying VZ, remained difficult to resolve and to clearly distinguish from the VZ using diffusion as a probe of cortical microstructure. It is also necessary to note that TDI contrasts provide visualization of tissue microstructure based on mapping of fiber density at subvoxel resolutions, but do not completely recover anatomical features that would be resolved with the acquisition of dMRI data at a native resolution equivalent to the grid size of the TDI maps, as shown by a previous validation study in the human brain by Calamante et al. (2011).

With the sample-averaged tensor contrasts generated by deformable registration of the dMRI data, we further examined regional changes in anisotropy in the developing cortex over the embryonic period. The averaged anisotropy maps revealed a marked spatio-temporal gradient of FA increase in the CP, with an associated reverse gradient of FA decrease in the VZ (Fig. 8). Although histogenetic changes during corticogenesis

in the mouse have been well documented in the past, our knowledge of regional variation in the microstructure across different cortical areas is relatively scarce, because histological studies have focused on specific regions of the cortex at a time. Using autoradiography of coronal sections, a previous study has shown that the wave of neuronal differentiation during corticogenesis proceeds in a ventrolateral to dorsomedial fashion along the cortical arc (Smart and Smart 1982). The sequence of neurogenesis and radial migration is also known to follow a transverse neurogenetic gradient, being initiated rostrolaterally and propagating caudomedially (Bayer and Altman 1991; Takahashi et al. 1999). These findings suggest that the observed spatio-temporal FA gradient coincides with the "wave front" of the initiation and termination of neurogenesis along the rostrolateral-to-caudomedial axis of the developing cortex. Interestingly, progressive loss of cortical anisotropy in the early postnatal rat brain has also been shown to follow a similar rostral to caudal gradient (Huang et al. 2008). However, more detailed histological analyses of the underlying cortical cytoarchitecture, and its regional variation across the cerebral wall, will be necessary in order to elucidate the precise microstructural changes that contribute to the observed spatio-temporal gradients of anisotropy in the VZ and the CP.

In this study, the dMRI data were acquired with sampling of 18 diffusion-weighted directions, which were chosen to acquire high spatial resolution data with a high SNR (~76–87) within a reasonable scan time. Recent studies have reported ultra high-resolution diffusion tensor microimaging of the mouse brain and nervous tissue (Aggarwal et al. 2010; Flint et al. 2010; Jiang and Johnson 2010). Here, using tensor-based contrasts, we investigated quantitative changes in regional anisotropy and its orientation in the embryonic cortex. Furthermore, using higher sampling directions relative to diffusion tensor-based acquisitions, spherical deconvolution of the dMRI data was used for probabilistic tractography and subvoxel mapping of TDI contrasts, which allowed finer structural features to be resolved. For example, both radial and tangential microstructures could be resolved apposed orthogonally in the developing IZ, which are difficult to visualize using tensor-based contrasts. Additionally, interdigitating tangential fibers in the IZ could be resolved as they fanned out into the radially oriented gray matter of the CP in later embryonic stages (Fig. 6). The number of excitations (and SNR) can also be traded in order to acquire a higher number (≥30) of diffusion directions for estimation of FOD functions up to higher harmonic orders, which could potentially reveal further anatomical detail in areas of complex crossing structural orientations.

In conclusion, our study demonstrated that microstructure of the developing cerebral cortex in the mouse embryo can be three-dimensionally examined with dMR microscopy. The findings of this work will be useful for investigations of genetically modified mouse models with cortical development defects. The precise temporal sequence of cortical development during the embryonic period established here will also serve as a baseline for anatomical phenotyping and screening of mutant models with cortical formation defects, and to direct further histological analyses to specific cortical regions.

Funding

This work was supported by the National Institutes of Health (grants R01AG020012 and R01EB003543 to S.M.) and National Health and Medical Research Council (NHMRC) (grants APP1043045 and APP1048849 to L.J.R.). L.J.R. is supported by an NHMRC Principal Research Fellowship.

Notes

Conflict of Interest: None declared.

References

Aggarwal M, Mori S, Shimogori T, Blackshaw S, Zhang J. 2010. Three-dimensional diffusion tensor microimaging for anatomical characterization of the mouse brain. Magn Reson Med. 64:249–261.

Aggarwal M, Zhang J, Miller MI, Sidman RL, Mori S. 2009. Magnetic resonance imaging and micro-computed tomography combined atlas of developing and adult mouse brains for stereotaxic surgery. Neuroscience. 162:1339–1350.

Alexander DC, Pierpaoli C, Basser PJ, Gee JC. 2001. Spatial transformations of diffusion tensor magnetic resonance images. IEEE Trans Med Imaging. 20:1131–1139.

Angevine JB Jr, Sidman RL. 1961. Autoradiographic study of cell migration during histogenesis of cerebral cortex in the mouse. Nature. 192:766–768.

Austin CP, Cepko CL. 1990. Cellular migration patterns in the developing mouse cerebral cortex. Development. 110:713–732.

Baloch S, Verma R, Huang H, Khurd P, Clark S, Yarowsky P, Abel T, Mori S, Davatzikos C. 2009. Quantification of brain maturation and growth patterns in C57BL/6J mice via computational neuroanatomy of diffusion tensor images. Cereb Cortex. 19:675–687.

Bayer SA, Altman J. 1991. Neocortical development. New York: Raven Press.

Beaulieu C. 2002. The basis of anisotropic water diffusion in the nervous system—a technical review. NMR Biomed. 15:435–455.

Behrens TE, Johansen-Berg H, Woolrich MW, Smith SM, Wheeler-Kingshott CA, Boulby PA, Barker GJ, Sillery EL, Sheehan K, Ciccarelli O et al. 2003. Non-invasive mapping of connections between human thalamus and cortex using diffusion imaging. Nat Neurosci. 6:750–757.

Calamante F, Tournier JD, Heidemann RM, Anwander A, Jackson GD, Connelly A. 2011. Track density imaging (TDI): validation of super resolution property. NeuroImage. 56:1259–1266.

Calamante F, Tournier JD, Kurniawan ND, Yang Z, Gyengesi E, Galloway GJ, Reutens DC, Connelly A. 2012. Super-resolution track-density imaging studies of mouse brain: comparison to histology. NeuroImage. 59:286–296.

Chung K, Wallace J, Kim SY, Kalyanasundaram S, Andalman AS, Davidson TJ, Mirzabekov JJ, Zalocusky KA, Mattis J, Denisin AK et al. 2013. Structural and molecular interrogation of intact biological systems. Nature. 497:332–337.

Dehay C, Kennedy H. 2007. Cell-cycle control and cortical development. Nat Rev Neurosci. 8:438–450.

Del Rio JA, Martinez A, Auladell C, Soriano E. 2000. Developmental history of the subplate and developing white matter in the murine neocortex. Neuronal organization and relationship with the main afferent systems at embryonic and perinatal stages. Cereb Cortex. 10:784–801.

Dodt HU, Leischner U, Schierloh A, Jahrling N, Mauch CP, Deininger K, Deussing JM, Eder M, Zieglgansberger W, Becker K. 2007. Ultramicroscopy: three-dimensional visualization of neuronal networks in the whole mouse brain. Nat Methods. 4:331–336.

Flint JJ, Hansen B, Fey M, Schmidig D, King MA, Vestergaard-Poulsen P, Blackband SJ. 2010. Cellular-level diffusion tensor microscopy and fiber tracking in mammalian nervous tissue with direct histological correlation. NeuroImage. 52:556–561.

Hirst E, Asante J, Price J. 1991. Clustering of dendrites in the cerebral cortex begins in the embryonic cortical plate. J Neurocytol. 20:431–438.

Huang H, Xue R, Zhang J, Ren T, Richards LJ, Yarowsky P, Miller MI, Mori S. 2009. Anatomical characterization of human fetal brain development with diffusion tensor magnetic resonance imaging. J Neurosci. 29:4263–4273.

Huang H, Yamamoto A, Hossain MA, Younes L, Mori S. 2008. Quantitative cortical mapping of fractional anisotropy in developing rat brains. J Neurosci. 28:1427–1433.
Jacobs RE, Ahrens ET, Dickinson ME, Laidlaw D. 1999. Towards a microMRI atlas of mouse development. Comput Med Imaging Graph. 23:15–24.
Jiang H, van Zijl PCM, Kim J, Pearlson GD, Mori S. 2006. DtiStudio: resource program for diffusion tensor computation and fiber bundle tracking. Comput Methods Programs Biomed. 81:106–116.
Jiang Y, Johnson GA. 2010. Microscopic diffusion tensor imaging of the mouse brain. NeuroImage. 50:465–471.
Kolasinski J, Takahashi E, Stevens AA, Benner T, Fischl B, Zollei L, Grant PE. 2013. Radial and tangential neuronal migration pathways in the human fetal brain: anatomically distinct patterns of diffusion MRI coherence. NeuroImage. 79:412–422.
Kostovic I, Judas M, Rados M, Hrabac P. 2002. Laminar organization of the human fetal cerebrum revealed by histochemical markers and magnetic resonance imaging. Cereb Cortex. 12:536–544.
Kroenke CD, Bretthorst GL, Inder TE, Neil JJ. 2005. Diffusion MR imaging characteristics of the developing primate brain. NeuroImage. 25:1205–1213.
Kroenke CD, Van Essen DC, Inder TE, Rees S, Bretthorst GL, Neil JJ. 2007. Microstructural changes of the baboon cerebral cortex during gestational development reflected in magnetic resonance imaging diffusion anisotropy. J Neurosci. 27:12506–12515.
Kwan KY, Sestan N, Anton ES. 2012. Transcriptional co-regulation of neuronal migration and laminar identity in the neocortex. Development. 139:1535–1546.
McKinstry RC, Mathur A, Miller JH, Ozcan A, Snyder AZ, Schefft GL, Almli CR, Shiran SI, Conturo TE, Neil JJ. 2002. Radial organization of developing preterm human cerebral cortex revealed by noninvasive water diffusion anisotropy MRI. Cereb Cortex. 12:1237–1243.
Miller MI, Trouve A, Younes L. 2002. On the metrics and Euler-Lagrange equations of computational anatomy. Ann Rev Biomed Eng. 4:375–405.
Miyama S, Takahashi T, Nowakowski RS, Caviness VS Jr. 1997. A gradient in the duration of the G1 phase in the murine neocortical proliferative epithelium. Cereb Cortex. 7:678–689.
Mori S, Itoh R, Zhang J, Kaufmann WE, van Zijl PC, Solaiyappan M, Yarowsky P. 2001. Diffusion tensor imaging of the developing mouse brain. Magn Reson Med. 46:18–23.
Mori S, van Zijl PCM. 1998. A motion correction scheme by twin-echo navigation for diffusion weighted magnetic resonance imaging with multiple RF echo acquisition. Magn Reson Med. 40:511–516.
Noctor SC, Flint AC, Weissman TA, Dammerman RS, Kriegstein AR. 2001. Neurons derived from radial glial cells establish radial units in neocortex. Nature. 409:714–720.
Parker GJ, Haroon HA, Wheeler-Kingshott CA. 2003. A framework for a streamline-based probabilistic index of connectivity (PICo) using a structural interpretation of MRI diffusion measurements. J Magn Reson Imaging. 18:242–254.
Plachez C, Lindwall C, Sunn N, Piper M, Moldrich RX, Campbell CE, Osinski JM, Gronostajski RM, Richards LJ. 2008. Nuclear factor I gene expression in the developing forebrain. J Comp Neurol. 508:385–401.
Rakic P. 1982. Early developmental events: cell lineages, acquisition of neuronal positions, and areal and laminar development. Neurosci Res Program Bull. 20:439–451.
Rakic P. 1972. Mode of cell migration to the superficial layers of fetal monkey neocortex. J Comp Neurol. 145:61–83.
Schmid RS, McGrath B, Berechid BE, Boyles B, Marchionni M, Sestan N, Anton ES. 2003. Neuregulin 1-erbB2 signaling is required for the establishment of radial glia and their transformation into astrocytes in cerebral cortex. Proc Natl Acad Sci USA. 100:4251–4256.
Sidman RL, Rakic P. 1973. Neuronal migration, with special reference to developing human brain: a review. Brain Res. 62:1–35.
Smart IH. 1983. Three dimensional growth of the mouse isocortex. J Anat. 137(Pt 4):683–694.
Smart IH, McSherry GM. 1982. Growth patterns in the lateral wall of the mouse telencephalon. II. Histological changes during and subsequent to the period of isocortical neuron production. J Anat. 134:415–442.
Smart IH, Smart M. 1982. Growth patterns in the lateral wall of the mouse telencephalon: I. Autoradiographic studies of the histogenesis of the isocortex and adjacent areas. J Anat. 134:273–298.
Takahashi T, Goto T, Miyama S, Nowakowski RS, Caviness VS Jr. 1999. Sequence of neuron origin and neocortical laminar fate: relation to cell cycle of origin in the developing murine cerebral wall. J Neurosci. 19:10357–10371.
Tournier JD, Calamante F, Connelly A. 2012. MRtrix: diffusion tractography in crossing fiber regions. Int J Imaging Syst Technol. 22:53–66.
Turnbull DH, Mori S. 2007. MRI in mouse developmental biology. NMR Biomed. 20:265–274.
Westin CF, Maier SE, Mamata H, Nabavi A, Jolesz FA, Kikinis R. 2002. Processing and visualization for diffusion tensor MRI. Med Image Anal. 6:93–108.
Wong MD, Dorr AE, Walls JR, Lerch JP, Henkelman RM. 2012. A novel 3D mouse embryo atlas based on micro-CT. Development. 139:3248–3256.
Woods RP, Grafton ST, Holmes CJ, Cherry SR, Mazziotta JC. 1998. Automated image registration: I. General methods and intrasubject, intramodality validation. J Comput Assist Tomogr. 22:139–152.
Xu G, Takahashi E, Folkerth RD, Haynes RL, Volpe JJ, Grant PE, Kinney HC. 2014. Radial coherence of diffusion tractography in the cerebral white matter of the human fetus: neuroanatomic insights. Cereb Cortex. 24:579–592.
Zhang J, Richards LJ, Yarowsky P, Huang H, van Zijl PC, Mori S. 2003. Three-dimensional anatomical characterization of the developing mouse brain by diffusion tensor microimaging. NeuroImage. 20:1639–1648.